

# Lawrence Berkeley National Laboratory

## LBL Publications

### Title

Precision measurement of the  $\alpha$  particle magnetic moment  
`\documentclass[12pt]{minimal} \usepackage{amsmath}`  
`\usepackage{wasysym} \usepackage{amsfonts} \usepackage{amssymb}`  
`\usepackage{amsbsy} \usepackage{mathrsfs} \usepackage{upgreek}`  
`\setlength{\oddsidemargin}{-69pt} \begin{do...`

### Permalink

<https://escholarship.org/uc/item/4082n84j>

### Journal

European Physical Journal C, 12(1)

### ISSN

1434-6044

### Authors

The NA48 Collaboration  
Fanti et al., V

### Publication Date

2000

### DOI

10.1007/s100529900232

Peer reviewed

# Precision measurement of the $\Xi^0$ mass and the branching ratios of the decays $\Xi^0 \rightarrow \Lambda\gamma$ and $\Xi^0 \rightarrow \Sigma^0\gamma$

The NA48 Collaboration

V. Fanti, A. Lai, D. Marras, L. Musa, A. Nappi<sup>a</sup>

Dipartimento di Fisica dell'Università e Sezione dell'INFN di Cagliari, 09100 Cagliari, Italy

B. Hay, K.N. Moore<sup>b</sup>, R.W. Moore<sup>b</sup>, D.J. Munday, M.D. Needham<sup>c</sup>, M.A. Parker, T.O. White, S.A. Wotton  
Cavendish Laboratory, University of Cambridge<sup>d</sup>, Cambridge CB3 0HE, UK

G. Barr, H. Blümer<sup>e</sup>, G. Bocquet, J. Bremer, A. Ceccucci<sup>f</sup>, J. Cogan, D. Cundy, N. Doble, G. Fischer<sup>g</sup>, W. Funk, L. Gagnon, A. Gianoli<sup>h</sup>, A. Gonidec, G. Govi, P. Grafström, A. Lacourt, S. Luitz<sup>i</sup>, V. Marzulli, J.P. Matheys, A. Norton, S. Palestini<sup>f</sup>, B. Panzer-Steindel, D. Schinzel, H. Taureg, M. Velasco, O. Vossnack, H. Wahl, G. Wirrer  
CERN, 1211 Geneva 23, Switzerland

A. Gaponenko, V. Kekelidze, D. Madigojine, A. Mestvirishvili<sup>a</sup>, N. Molokanova, Yu. Potrebenikov, G. Tatishvili, A. Tkatchev, A. Zinchenko

Joint Institute for Nuclear Research, Dubna, Russian Federation

O. Boyle, I.G. Knowles, V.J. Martin, H. Parsons

Department of Physics and Astronomy, University of Edinburgh<sup>d</sup>, JCMB King's Buildings, Mayfield Road, Edinburgh EH9 3JZ, UK

M. Contalbrigo, P. Dalpiaz, J. Duclos, A. Formica<sup>j</sup>, P.L. Frabetti<sup>k</sup>, M. Martini, F. Petrucci, M. Savrie  
Dipartimento di Fisica dell'Università e Sezione dell'INFN di Ferrara, 44100 Ferrara, Italy

A. Bizzeti<sup>l</sup>, M. Calvetti, G. Collazuol, G. Graziani, E. Iacopini, M. Lenti<sup>m</sup>, A. Michetti, C. Talamonti<sup>n</sup>  
Dipartimento di Fisica dell'Università e Sezione dell'INFN di Firenze, 50125 Firenze, Italy

H.G. Becker, D. Coward<sup>i</sup>, C. Ebersberger, H. Fox, A. Kalter, K. Kleinknecht, U. Koch, L. Köpke, B. Renk, J. Scheidt, J. Schmidt, Y. Schue, V. Schönharting, R. Wilhelm, M. Wittgen  
Institut für Physik, Universität Mainz<sup>o</sup>, 55099 Mainz, Germany

J.C. Chollet, S. Crépé, L. Fayard, L. Iconomidou-Fayard, J. Ocariz<sup>p</sup>, G. Unal, I. Wingerter  
Laboratoire de l'Accélérateur Linéaire, IN2P3-CNRS, Université de Paris-Sud, 91406 Orsay<sup>q</sup>, France

G. Anzivino, P. Cenci, P. Lubrano, M. Pepe

Dipartimento di Fisica dell'Università e Sezione dell'INFN di Perugia, 06100 Perugia, Italy

P. Calafiura<sup>r</sup>, R. Carosi, R. Casali, C. Cerri, M. Cirilli, F. Costantini, R. Fantechi, S. Giudici, B. Gorini, I. Mannelli, G. Pierazzini, M. Sozzi

Dipartimento di Fisica, Scuola Normale Superiore e Sezione INFN di Pisa, 56100 Pisa, Italy

J.B. Cheze, M. De Beer, P. Debu, R. Granier de Cassagnac, P. Hristov<sup>s</sup>, E. Mazzucato, B. Peyaud, S. Schanne, R. Turlay, B. Vallage

DSM/DAPNIA - CEA-Saclay, 91191 Gif-sur-Yvette, France

I. Augustin, M. Bender, M. Holder, M. Ziolkowski

Fachbereich Physik, Universität Siegen<sup>t</sup>, 57068 Siegen, Germany

R. Arcidiacono, C. Biino, R. Cester, F. Marchetto, E. Menichetti, N. Pastrone

Dipartimento di Fisica Sperimentale dell'Università e Sezione dell'INFN di Torino, 10125 Torino, Italy

J. Nassalski, E. Rondio, M. Szleper, W. Wislicki, S. Wronka

Soltan Institute for Nuclear Studies, Laboratory for High Energy Physics<sup>u</sup>, 00-681 Warsaw, Poland

H. Dibon, M. Jeitler<sup>v</sup>, M. Markytan, I. Mikulec, G. Neuhofer, M. Pernicka, A. Taurok

Österreichische Akademie der Wissenschaften, Institut für Hochenergiephysik, 1050 Wien, Austria

Received: 6 August 1999 / Published online: 14 October 1999

**Abstract.** A new precision measurement of the  $\Xi^0$  mass has been performed at the NA48 experiment at the CERN SPS. The value obtained is  $[1314.82 \pm 0.06 \text{ (stat.)} \pm 0.2 \text{ (syst.)}] \text{ MeV}/c^2$ . The branching ratios of  $\Xi^0$  radiative decays have been measured as:  $\text{Br}(\Xi^0 \rightarrow \Lambda\gamma) = [1.90 \pm 0.34 \text{ (stat.)} \pm 0.19 \text{ (syst.)}] \cdot 10^{-3}$  and  $\text{Br}(\Xi^0 \rightarrow \Sigma^0\gamma) = [3.14 \pm 0.76 \text{ (stat.)} \pm 0.32 \text{ (syst.)}] \cdot 10^{-3}$ .

## 1 Introduction

A precise measurement of hyperon masses permits the checking of the mass splitting related to radiative corrections. The mass of the  $\Xi^0$  hyperon is known with less pre-

<sup>a</sup> Present address: Dipartimento di Fisica dell'Università e Sezione dell'INFN di Perugia, 06100 Perugia, Italy.

<sup>b</sup> Present address: Physics-Astronomy Building, Michigan State University, East Lansing, MI 48824 USA.

<sup>c</sup> Present address: NIKHEF, PO Box 41882,1009 DB Amsterdam, The Netherlands.

<sup>d</sup> Funded by the UK Particle Physics and Astronomy Research Council.

<sup>e</sup> Present address: Institute für Physik, Karlsruhe, Germany.

<sup>f</sup> Permanent address: Dipartimento di Fisica Sperimentale dell'Università e Sezione dell'INFN di Torino, 10125 Torino, Italy.

<sup>g</sup> Present address: Österreichische Akademie der Wissenschaften, Institut für Hochenergiephysik, 1050 Wien, Austria.

<sup>h</sup> Present address: Dipartimento di Fisica dell'Università e Sezione dell'INFN di Ferrara, 44100 Ferrara, Italy.

<sup>i</sup> Present address: SLAC, Stanford, CA 94309, USA.

<sup>j</sup> Present address: DSM/DAPNIA - CEA-Saclay, 91191 Gif-sur-Yvette, France.

<sup>k</sup> Permanent address: Dipartimento di Fisica e INFN, Bologna, Italy.

<sup>l</sup> Also at Dipartimento di Fisica dell'Università di Modena, Modena, Italy.

<sup>m</sup> Present address: CERN, 1211 Geneva 23, Switzerland.

<sup>n</sup> Present address: University of Florence, Department of Clinical Physiopathology, Italy.

<sup>o</sup> Funded by the German Federal Minister for Research and Technology (BMBF) under contract 7MZ18P(4)-TP2, Germany.

<sup>p</sup> Permanent address: Departamento de Física, Universidad de los Andes, Mérida 5101-A, Venezuela.

<sup>q</sup> Funded by Institut National de Physique des Particules et de Physique Nucléaire (IN2P3), France.

<sup>r</sup> Present address: Lawrence Berkeley National Laboratory, Berkeley, CA 94720 USA.

<sup>s</sup> Present address: Joint Institute for Nuclear Research, Dubna, Russian Federation.

<sup>t</sup> Funded by the German Federal Minister for Research and Technology (BMBF) under contract 056SI74, Germany.

<sup>u</sup> Supported by the Committee for Scientific Research (KBN) grant 2P03B07615 and using computing resources of the Interdisciplinary Center for Mathematical and Computational Modelling of the University of Warsaw.

<sup>v</sup> Funded by the Austrian Ministry for Research and Traffic under the contract GZ 616.363/2-VIII, Austria.

cision [2–5] than the other members of the  $SU(3)_{flavour}$  baryon octet. Thus, a precise measurement of the  $\Xi^0$  mass can contribute to a critical test of various theoretical approaches [6–9] to the mass calculations.

The transitions between the octet member states via radiative decays are allowed through U-spin conservation in the framework of  $SU(3)$  symmetry. The octet members  $\Sigma^0$  and  $\Lambda$  represent orthogonal three-quark-states with different U-spins. So the study of radiative decays like  $\Xi^0 \rightarrow \Lambda\gamma$  and  $\Xi^0 \rightarrow \Sigma^0\gamma$  gives information about the hyperon structure related to  $SU(3)$  violation. Theoretical predictions for the branching ratios of  $\Xi^0$  radiative decays deal with non-leptonic weak interactions and estimate hadronic effects and electromagnetic corrections. Difficulties in such calculations lead to results which range over almost two orders of magnitude [10–21]. There are several experiments [22–25] which measured these branching ratios, but only two of them [24,25] have adequate precision.

In the present work the mass of the  $\Xi^0$  hyperon has been precisely measured via the decay

$$\Xi^0 \rightarrow \Lambda\pi^0. \quad (1)$$

The radiative decays

$$\Xi^0 \rightarrow \Lambda\gamma, \quad (2)$$

and

$$\Xi^0 \rightarrow \Sigma^0\gamma \quad (3)$$

have been observed and their branching ratios measured. These measurements have been performed in the NA48 experiment at the CERN SPS.

## 2 Experimental set-up and data taking

The NA48 experiment is designed to measure direct CP violation in neutral kaon decays [26]. The  $K_S$  beam [27] contains  $K^0$  mesons and hyperons<sup>1</sup>. It is produced on a 0.2 cm diameter, 40 cm long beryllium target by 450-GeV protons. The protons are focused by a series of four quadrupole magnets and deflected by a dipole magnet to the target 7.2 cm above the initial proton beam axis, which points horizontally towards the detector. The set-up is described in a right-handed orthogonal coordinate system with the OZ- and OY-axes horizontal (along the initial

<sup>1</sup> This is one of the two simultaneous beams of the NA48 experiment: the  $K_S$  and  $K_L$  beams

proton beam axis) and vertical, respectively. The neutral beam has a production angle of 4.2 mrad [28,29]. The target is positioned at  $z=0$ , and followed by a sweeping magnet packed with tungsten-alloy inserts in which the protons not interacting in the target are absorbed, and by a 0.36 cm diameter collimator defining a downward direction of 0.6 mrad at  $z=4.8$  m. The 1.2 m long collimator is followed successively by an anti-counter (AKS), an 88 m long evacuated tube and by a helium-filled tank which contains the drift chambers. The AKS is formed by a set of three scintillation counters preceded by an aligned 3 mm thick iridium crystal and is used to veto decays occurring upstream the AKS. Decays occurring downstream the AKS in the upstream part of the evacuated region are accepted. The outer diameter of each of the sub-detectors is typically 2.5 m.

The present analysis is based on data recorded during the 42-day run in 1997 with a proton intensity of about  $3 \times 10^7$  protons hitting the target during the 2.4 s long SPS spill. Detector elements used for the present analysis are the following:

- A magnetic spectrometer used to measure tracks of charged particles. It includes two drift chambers upstream and two downstream a dipole magnet with the magnetic field directed vertically along the OY-axis that produces a 267 MeV/c transverse momentum kick. Each drift chamber [30] is composed of four double planes with staggered wires to resolve left-right ambiguities. The wire orientations in the four views are horizontal, vertical and  $\pm 45^\circ$  with respect to the horizontal/vertical plane (horizontal and vertical only in chamber 3). The average efficiency per plane is 99.5%. The resolution of a coordinate in a single chamber is 110  $\mu\text{m}$  and the mean momentum resolution of the four-chamber spectrometer is  $\delta p/p \simeq 0.6\%$  at 45 GeV/c.
- A liquid-krypton calorimeter (LKr) [31] is used to measure energy, position and timing of electromagnetic showers initiated by photons ( $\gamma$ ). Around 20 t of liquid krypton at 121 K are used as an ionization detector. The high density of krypton with its small Moliere radius (4.7 cm) provides a good separation of electromagnetic showers. The calorimeter has a structure of 13212 square towers of  $2 \times 2 \text{ cm}^2$  cross section and 127 cm length (27 radiation lengths) each. The cells are formed by copper-beryllium ribbons, 1.8 cm wide and 40  $\mu\text{m}$  thick, stretched longitudinally. The ionization signal from each of the cells is integrated, amplified, shaped, and digitized by 10-bit FADCs at 40 MHz sampling frequency [32]. The energy resolution is

$$\sigma(E)/E \simeq 0.125/E \oplus 0.032/\sqrt{E} \oplus 0.005,$$

where E is in GeV. The read-out system was calibrated by a charge pulse offered every burst during data taking. The final calibration of the energy scale is fixed by the fit of the AKS position using the  $K_S \rightarrow \pi^0 \pi^0$  decays. The relative calibrations of the individual cells were done using  $K_{e3}$  decays and  $\eta$  decays into  $3\pi$  and  $2\gamma$ 's. The position and time resolutions for a single

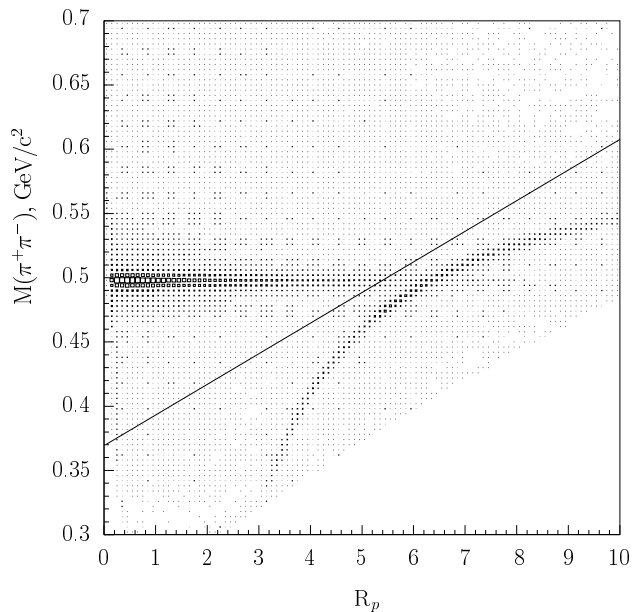


**Fig. 1.** Distribution of invariant mass  $M(\pi^+\pi^-)$  versus the momentum ratio of positive to negative tracks,  $R_p$

photon are better than 1.3 mm and 300 ps, respectively.

- A scintillator hodoscope located in front of the calorimeter is used for triggering on charged particles.
- A sampling hadron calorimeter composed of 48 steel plates, each 24 mm thick, interleaved with scintillator planes is designed to measure hadronic showers with a readout in horizontal and vertical projection. A fast energy sum from the calorimeter is used in the trigger.
- A muon veto system consisting of three planes of plastic scintillator, with an 80 cm thick iron wall in front of each plane is used to identify muons.

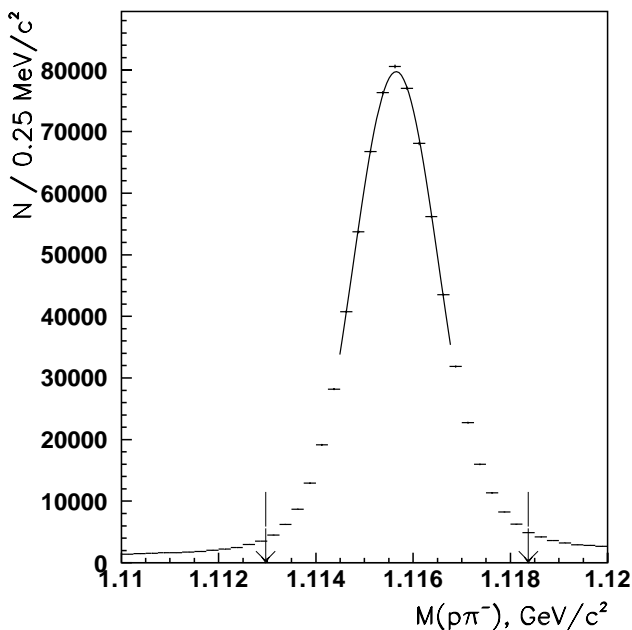
The data for the present analysis were recorded with a two-particle trigger. This trigger requires that events must have at least two hits in opposite quadrants of the charged hodoscope and an energy deposition in both calorimeters greater than 30 GeV.

A more complete description of the apparatus can be found elsewhere [33,34]. The analysis is described in [35].

### 3 Event selection

Decays of  $\Xi^0$ 's are selected by choosing events with one  $\Lambda$  and at least one  $\gamma$ . The  $\Lambda$  hyperons have been identified via their decays  $\Lambda \rightarrow p\pi^-$  using only the magnetic spectrometer, with a vertex reconstructed as the point  $(V_X, V_Y, V_Z)$  of closest distance of approach (CDA) of the two tracks. The following criteria have been applied for the  $\Lambda$  candidate selection:

- $CDA < 2.2$  cm which corresponds to three times the resolution on this parameter;
- $5 \text{ m} < V_Z < 40 \text{ m}$  and  $V_Y > 4$  cm defining the decay region of  $\Lambda$ 's produced in the neutral beam (the

Fig. 2. Spectrum of  $p\pi^-$  invariant mass

corresponding resolutions are 90 cm and 0.25 cm, respectively);

- the total momentum of the two charged particles must be greater than 57 GeV/c.

Fig. 1 shows the distribution of invariant mass of the two charged particles,  $M(\pi^+\pi^-)$ , and the momentum ratio of positive to negative particles ( $R_p$ ) in each selected event, under the assumption that both particles are pions. There is a significant fraction of  $K_S \rightarrow \pi^+\pi^-$  events as shown by the concentration at  $M(\pi^+\pi^-)$  of approximately 500 MeV/c<sup>2</sup>. Similarly, with this assumption, the kinematics of  $\Lambda \rightarrow p\pi^-$  yield the curved distribution in  $R_p$  over a wide range of  $M(\pi^+\pi^-)$ . To separate  $\Lambda$  decays from  $K_S$  decays, the following condition has been applied:

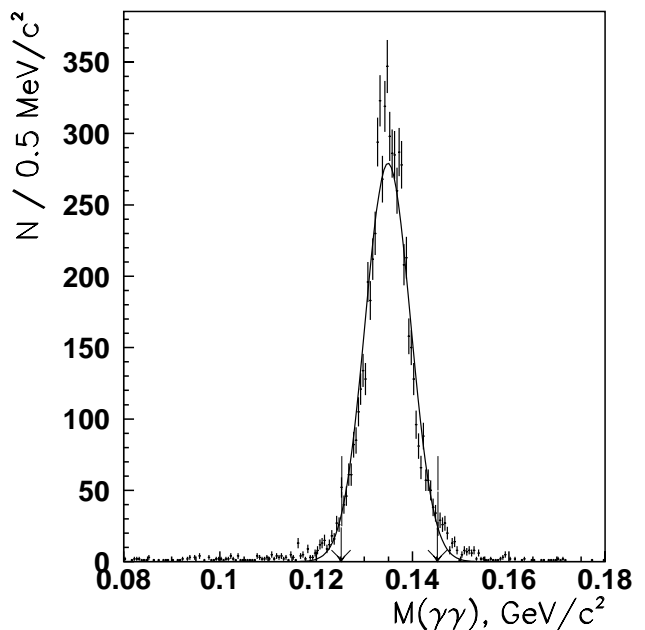
$$M(\pi\pi) \leq 0.37\text{GeV}/c^2 + R_p \cdot 0.024\text{GeV}/c^2,$$

which corresponds to the straight line in Fig. 1.

The invariant mass spectrum of the  $p\pi^-$  system,  $M(p\pi^-)$ , for the events selected according to the criteria above, is presented in Fig. 2. In this analysis, positively-charged particles are assumed to be protons and negatively-charged ones are taken to be pions. The  $\Lambda$  mass peak in this plot has been fit by a Gaussian distribution. The mean value of the mass,  $(1115.650 \pm 0.072)$  MeV/c<sup>2</sup>, is in good agreement with the nominal value of  $\Lambda$  mass [1]. The width of the signal is  $(0.90 \pm 0.03)$  MeV/c<sup>2</sup>. For the following analysis  $\Lambda$ 's were selected by requiring  $M(p\pi)$  to be within  $\pm 2.7$  MeV/c<sup>2</sup> from the nominal  $\Lambda$  mass [1].

The photons were identified using LKr clusters not associated with charged particle tracks. Clusters are characterized by deposited energy and the central position of the shower. The following criteria have been applied for the selection of  $\gamma$  rays associated with the events:

- the cluster center is positioned not closer than 25 cm from the impact point of each of the tracks; this is

Fig. 3. Spectrum of  $M(\gamma\gamma)$ 

required in order to separate electromagnetic showers from possible hadronic shower fluctuations;

- the cluster energy is greater than 6 GeV to reject  $\gamma$ 's from bremsstrahlung arising from electrons or positrons;
- the cluster time is within  $\pm 3$  ns from the mean event time to reject clusters of accidental events;
- the cluster center is at least 15 cm outside the beam pipe axis.

The  $\Xi^0$  flight trajectory is reconstructed as a vector originating at the target center and directed to the point of the ‘‘center of gravity’’ (COG) on the front face of the LKr. The x and y coordinates of the COG are calculated as the mean values of the corresponding coordinates of all charged particles and photons, weighted by their energies. The divergence of the  $\Xi^0$  beam is limited by the collimator, but has been additionally restricted by the requirement that the COG to be inside a radius of  $< 7$  cm in order to avoid possible ‘‘edge effects’’ on the collimator.

The  $\Xi^0$  decay vertex is defined as the point ( $V'_X, V'_Y, V'_Z$ ) of closest distance of approach of the reconstructed trajectories of the  $\Xi^0$  and  $\Lambda$  hyperons. A typical resolution on  $V'_Z$ , is around 230 cm.

The selected sample has 62300 events containing one  $\Lambda$  hyperon and at least one photon.

#### 4 $\Xi^0 \rightarrow \Lambda\pi^0$ decay reconstruction

To reconstruct  $\Xi^0 \rightarrow \Lambda\pi^0$  decays, 13532 events containing a  $\Lambda$  hyperon and at least two  $\gamma$ 's selected according to the criteria mentioned above have been analyzed (very few of these events have more than two photons). As the first approximation the  $2\gamma$  invariant mass  $M(\gamma\gamma)$  was reconstructed under the assumption that the  $\pi^0 \rightarrow \gamma\gamma$  decay

occurs at  $(V'_X, V'_Y, V'_Z)$ , i.e. at the  $\Xi^0$  decay vertex discussed above. The spectrum of  $M(\gamma\gamma)$  obtained under this assumption is plotted in Fig. 3 and shows a clear  $\pi^0$  signal. A normal distribution fit to the signal gives a mean value ( $134.49 \text{ MeV}/c^2$ ) in good agreement with the nominal  $\pi^0$  mass [1], and a width of  $4.30 \pm 0.06 \text{ MeV}/c^2$ . The pairs of  $\gamma$ 's with

$$125 \text{ MeV}/c^2 < M(\gamma\gamma) < 145 \text{ MeV}/c^2$$

are selected as  $\pi^0 \rightarrow \gamma\gamma$  decays. After applying this criterion 6669 events have been left, all of which were identified with the  $\Xi^0 \rightarrow \Lambda\pi^0$  decays, because the appropriate distribution of the  $\Lambda\pi^0$  invariant mass,  $M(\Lambda\pi^0)$ , shows an explicit peak centered at the  $\Xi^0$  nominal mass.

To diminish systematics in the  $M(\Lambda\pi^0)$  measurement related with the uncertainties of the geometry and energy scale definition, the following corrections and selection criterion have been implemented. The z-coordinate of the  $\pi^0$  decay vertex,  $z_{\pi^0}$ , has been calculated using the nominal  $\pi^0$  mass,  $m_{\pi^0}$ , in the expression:

$$z_{cal} - z_{\pi^0} = \sqrt{E_1 E_2 [(x_1 - x_2)^2 + (y_1 - y_2)^2]} / m_{\pi^0},$$

where  $z_{cal}$  is the z-coordinate of the front face of the LKr calorimeter,  $E_i$  is the energy of the i-th photon, and  $x_i$  and  $y_i$  are respectively x and y coordinates of the i-th photon impact point to the LKr calorimeter. Only those events have been selected which have no large difference between the two vertexes:

$$|V'_z - z_{\pi^0}| \leq 300 \text{ cm}.$$

For the  $\Xi^0$  decay vertex the point has been taken on the  $\Lambda$  trajectory at  $z_{\pi^0}$ . In addition, the invariant mass  $M(\Lambda\pi^0)$  was recalculated using the nominal masses [1] of the identified  $\Lambda$  and  $\pi^0$ . The spectrum of the obtained  $M(\Lambda\pi^0)$  is plotted in Fig. 4. The observed clear signal of  $\Xi^0$  decays (1) has been fit by a Gaussian distribution. The signal is due to 3120 events with a mean mass value of

$$M(\Xi^0) = [1314.82 \pm 0.06(stat.)] \text{ MeV}/c^2,$$

and a width equal to  $(1.10 \pm 0.04) \text{ MeV}/c^2$ .

The main systematic error in the  $\Xi^0$  mass measurement is caused by the uncertainty of the energy scale calibration in both, the spectrometer and LKr calorimeter. The energy scale is almost linearly related to the reconstructed position of the  $\Xi^0$  decay vertex. The difference between two vertexes,  $(V'_z - z_{\pi^0})$ , has been estimated with the precision of 30 cm. This value has been taken as the uncertainty in the reconstruction of the  $\Xi^0$  decay vertex. This uncertainty leads to a systematic error in the  $\Xi^0$  mass measurement of  $0.2 \text{ MeV}/c^2$ .

## 5 Measurement of $\Xi^0 \rightarrow \Lambda\gamma$ decay branching ratio

In order to select the radiative decay  $\Xi^0 \rightarrow \Lambda\gamma$ , the trajectories of  $\Xi^0$  and  $\Lambda$  have been reconstructed as described

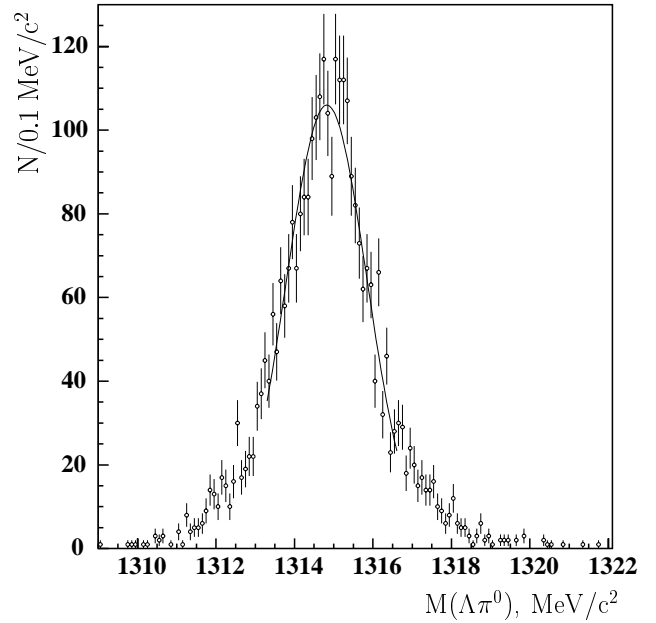


Fig. 4. Spectrum of  $\Lambda\pi^0$  invariant mass

in Sect. 3. The decay vertex  $(V'_X, V'_Y, V'_Z)$  has been found as a point of CDA of these two trajectories. The major background contribution to these decays is due to the  $\Xi^0 \rightarrow \Lambda\pi^0$  and  $\Xi^0 \rightarrow \Sigma^0\gamma$  decays in which one  $\gamma$  is not detected. Most of the background decays could be distinguished kinematically. The following criteria have been optimized by a Monte Carlo simulation for  $\Lambda\gamma$  events:

- the  $\gamma$  energy ( $E_\gamma$ ) has to be greater than 15 GeV;
- the distance ( $\Delta$ ) between the impact points on the front face of the LKr by the photon and any charged track, is larger than 30 cm;
- $5m < V'_Z < V_Z$ ;
- $V'_Z < 20 \text{ m}$  (because at higher  $V'_Z$  the background contribution increases significantly);
- the squared transverse momentum of the  $\Lambda\gamma$  system with respect to the  $\Xi^0$  trajectory ( $P_t^2$ ) is less than  $0.003 \text{ GeV}^2/c^2$  (three times the corresponding resolution).

After applying the above criteria 31 signal events have been left in the interval of the  $\Lambda\gamma$  invariant mass,  $M(\Lambda\gamma)$ , from  $1300 \text{ MeV}/c^2$  to  $1330 \text{ MeV}/c^2$  (Fig. 5a). The 32330 Monte Carlo simulated events which remained after the application of the same criteria (Fig. 5b) correspond to an acceptance value of  $A(\Lambda\gamma) = 6.74\% \pm 0.04\%(stat.)$ .

Possible background from decays according to reactions (1) and (3) have been estimated by the Monte Carlo simulation to 0.16 events.

Using the  $\text{Br}(\Xi^0 \rightarrow \Lambda\pi^0)$  as a normalization [1], for which the acceptance obtained with the Monte Carlo simulation is  $A(\Lambda\pi^0) = 2.765\% \pm 0.008\%(stat.)$ , the branching ratio of the radiative decay is:

$$\text{Br}(\Xi^0 \rightarrow \Lambda\gamma) = [1.90 \pm 0.34(stat.) \pm 0.19(syst.)] \cdot 10^{-3}.$$

The systematic error was estimated by varying the cuts on  $E_\gamma$ ,  $\Delta$ , and  $P_t^2$ .

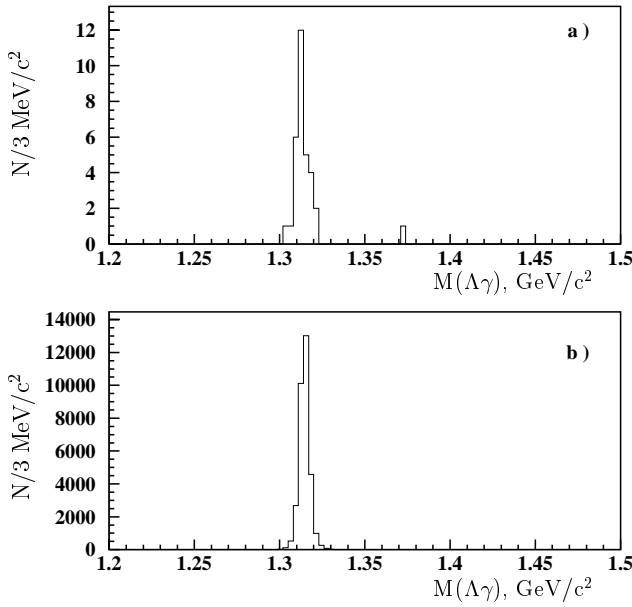


**Fig. 5a,b.** Invariant mass of  $M(\Lambda\gamma)$  for the  $\Xi^0 \rightarrow \Lambda\gamma$  decay candidates: **a** experimental data; **b** simulated events

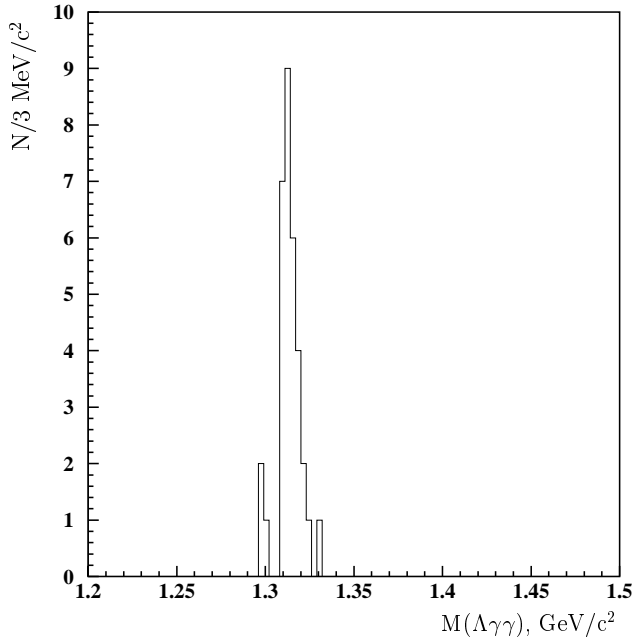


**Fig. 6.** Invariant mass of  $M(\Lambda\gamma\gamma)$  for candidates to  $\Xi^0 \rightarrow \Sigma^0\gamma$  decays

## 6 Measurement of $\Xi^0 \rightarrow \Sigma^0\gamma$ decay branching ratio

$\Xi^0 \rightarrow \Sigma^0\gamma$  decays have been selected from events containing one  $\Lambda$ 's and at least two  $\gamma$ 's. The  $\Xi^0$  and  $\Lambda$  trajectories and their vertices have been reconstructed as described in Sect. 3. The vertex of the secondary  $\Sigma^0 \rightarrow \Lambda\gamma$  decay is assumed to be the same as the  $\Xi^0$  decay vertex. Additional selection criteria are the following:

- $5m < V_Z' < V_Z$ ;

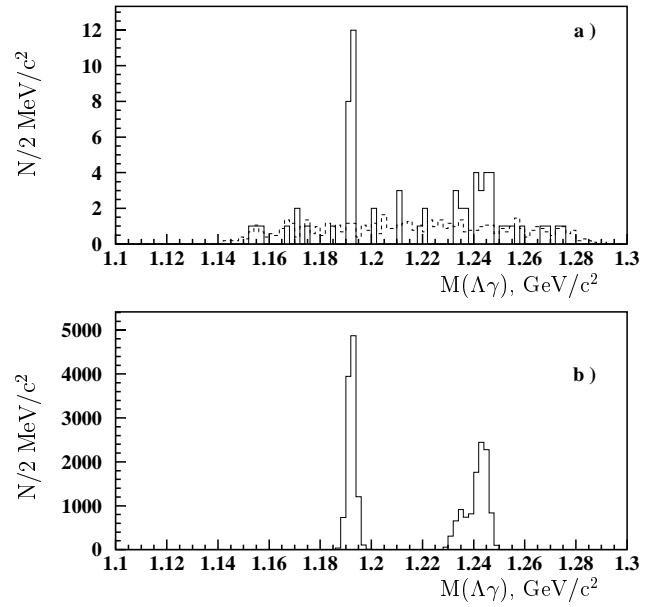


**Fig. 7a,b.** Invariant mass of  $M(\Lambda\gamma)$  for the  $\Sigma^0 \rightarrow \Lambda\gamma$  decay candidates: **a** experimental data (solid line) and simulated background from the  $\Xi^0 \rightarrow \Lambda\pi^0$  decays(dashed line); **b** simulated events

- $M(\gamma\gamma)$  outside the region of  $125 \text{ MeV}/c^2 \leq M(\gamma\gamma) \leq 145 \text{ MeV}/c^2$  to reject  $\pi^0$ .

The invariant mass of  $M(\Lambda\gamma\gamma)$  calculated using the  $\Lambda$  mass from [1] for the selected events is presented in Fig.6. The peak around the  $\Xi^0$  mass is due to decays of  $\Xi^0$  with  $\Lambda$  and two  $\gamma$ 's in the final state. Thirty-three events presented in this plot have been used to recalculate the z-coordinate of the  $\Xi^0$  decay vertex ( $V_Z''$ ). All these events have been considered as decays of  $\Xi^0$  and the nominal value of the  $\Xi^0$  mass [1] has been used to calculate  $V_Z''$  as the origin of the two photons. To check whether the observed final states are products of  $\Xi^0 \rightarrow \Sigma^0\gamma$  decays, these 33 events are plotted versus the invariant mass  $M(\Lambda\gamma)$  calculated using  $V_Z''$  (Fig. 7a). A clear signal of  $\Sigma^0 \rightarrow \Lambda\gamma$  decays is seen in this plot as well as a bump at higher mass caused by a wrong assignment of photons in each of the events. The signal is reliably separated from this bump. This separation has been confirmed by a Monte Carlo simulation of the relevant decays (Fig. 7b). To identify the  $\Sigma^0 \rightarrow \Lambda\gamma$  decays it was required, in accordance with the simulation, that the invariant mass of the  $\Lambda\gamma$  system  $M(\Lambda\gamma)$  should be in the range:  $1187.5 \text{ MeV}/c^2 < M(\Lambda\gamma) < 1197.5 \text{ MeV}/c^2$ .

The major background is expected to come from the  $\Xi^0 \rightarrow \Lambda\pi^0$  decays in which the  $\pi^0$ 's pass the rejection criteria on  $M(\gamma\gamma)$ . The background events simulated in this way agree well with the experimental distribution of the  $\Lambda\gamma$  invariant mass (dashed line in Fig. 7a). The estimated background from this process is  $(3.1 \pm 0.5)$  events.

Finally, 17 events have been identified as  $\Xi^0 \rightarrow \Sigma^0\gamma$  decays. The acceptance, estimated from the Monte Carlo



simulation, is:

$$A(\Xi^0 \rightarrow \Sigma^0 \gamma) = 2.24\% \pm 0.02\%(stat.).$$

Using the  $Br(\Xi^0 \rightarrow \Lambda \pi^0)$  as a normalization [1], the branching ratio for the radiative decay is obtained:

$$Br(\Xi^0 \rightarrow \Sigma^0 \gamma) = [3.14 \pm 0.76(stat.) \pm 0.32(syst.)] \cdot 10^{-3}.$$

The systematic error was estimated again by varying the cuts in the selection criteria on  $M(\gamma\gamma)$  and  $E_\gamma$ .

## 7 Conclusion

The  $\Xi^0$  hyperons produced by 450 GeV protons and decaying into  $\Lambda \pi^0$  (6669 events),  $\Lambda \gamma$  (31 events), and  $\Sigma^0 \gamma$  (17 events) have been observed in the NA48 experiment.

The  $\Xi^0$  mass has been measured as:

$$M(\Xi^0) = [1314.82 \pm 0.06(stat.) \pm 0.20(syst.)] \text{ MeV}/c^2$$

which is the most precise measurement of this mass so far. The other measurements and the mean value quoted in [1] are compatible with the present result within their accuracy.

Taking into account the mean value of the  $\Xi^-$  mass [1] a mass difference of  $M(\Xi^-) - M(\Xi^0) = (6.50 \pm 0.25) \text{ MeV}/c^2$  is obtained. This difference is more than 3 standard deviations higher than the result  $(5.68 \pm 0.24) \text{ MeV}/c^2$  calculated in the framework of Lattice QCD [7] and is within 2 standard deviations of the theoretical result of  $6.10 \text{ MeV}/c^2$  based on radiative corrections to the quark model [9].

The measured branching ratio:

$$Br(\Xi^0 \rightarrow \Sigma^0 \gamma) = [3.14 \pm 0.76(stat.) \pm 0.32(syst.)] \cdot 10^{-3}$$

agrees with the precise measurement performed in the FNAL experiment [24], while the other measured branching ratio:

$$Br(\Xi^0 \rightarrow \Lambda \gamma) = [1.90 \pm 0.34(stat.) \pm 0.19(syst.)] \cdot 10^{-3}$$

disagrees at the level of 2 standard deviations with the measurement done at FNAL [25].

The ratio of the two branching ratios is:

$$Br(\Xi^0 \rightarrow \Sigma^0 \gamma)/Br(\Xi^0 \rightarrow \Lambda \gamma) = 1.65 \pm 0.55.$$

The results obtained are compared with predictions of various theoretical models in Table 1<sup>2</sup>.

The comparison in this table shows that most of the model calculations cannot reproduce the obtained results; only the most recent calculation [20] based on SU(6) symmetry and vector meson dominance is in agreement with our results.

*Acknowledgements.* It is a pleasure to thank the staff of the participating laboratories, universities and affiliated computing centers for their efforts in the construction of the NA48 apparatus, the operation of the experiment, and the processing of the data.

<sup>2</sup> The errors indicated are obtained by adding in quadrature the corresponding statistical and systematic errors

**Table 1.** Comparison of our results with the theoretical predictions

Refer.	$Br(\Sigma^0 \gamma)/10^{-3}$	$Br(\Lambda \gamma)/10^{-3}$	$Br(\Sigma^0 \gamma)/Br(\Lambda \gamma)$
This Exp.	$3.14 \pm 0.82$	$1.90 \pm 0.39$	$1.65 \pm 0.55$
Models			
[11]	9.10	4.00	2.28
[13]	5.87	2.29	2.56
[14]	2.62	0.70	3.74
[15]	1.48	1.80	0.82
[20]	3.49	2.06	1.69

## References

1. Review of particle physics. *Eur. Phys. J. C*3 (1998) 1-794.
2. G.W.London et al., *Phys.Rev.* 143 (1966) 1034.
3. G.M.Pjerrou et al., *Phys.Rev.Lett.* 14 (1965) 275.
4. L.Jauneau et al., *Phys.Lett.* 4 (1963) 49.
5. G.Wilquet et al., *Phys.Lett.* B42 (1972) 372.
6. S.Coleman and S.L.Glashow, *Phys. Rev. Lett.* 6 (1961) 423.
7. A.Duncan, E.Eichten and H.Thacker, *Nucl. Phys. Proc. Suppl.* 53 (1997) 299-301.
8. J.L.Rosner, *EFI 97-33- Rev.* (1998).
9. R.Delbourgo et al., *Phys. Rev D*59 (1999) 113006.
10. M.Scadron and L.Thebaud, *Phys.Rev.* D8 (1973) 2190.
11. F.J.Gilman and A.B.Wise, *Phys.Rev.* D19 (1979) 976.
12. M.B.Gavela et al., *Phys.Lett.* B101 (1981) 417.
13. K.G.Rauh, *Z. Phys. Rev.* C10 (1981) 81.
14. R.C.Verma and A.Sharma, *Phys.Rev.* D38 (1988) 1443.
15. A.N.Kamal and R.C. Verma, *Phys.Rev.* D26 (1982) 190.
16. Riazuddin and Fayazuddin, *International Center for Theoretical Physics, Trieste*, Report No.IC/79/54 (1979).
17. P.Eckert and B.Morel, *Geneva University Report No UGVA-DPT 1982/03-340* (1982).
18. W.F.Kao and H.J.Schnitzer, *Phys.Lett.* B183 (1987) 361; *Phys.Rev.* D37 (1988) 1912.
19. G.Nardulli, *Nuovo Cimento*, 100A (1988) 485.
20. P.Zenczykowski, *Phys.Rev.* D40 (1989) 2290.
21. M. Gaillard et al. *Phys. Lett.* B158 (1985) 8.
22. T.Yeh et al., *Phys.Rev.* D10 (1974) 3545.
23. J.R.Besinger et al., *Phys. Lett.* B215 (1988) 195.
24. S.Teige et al., *Phys.Rev.Lett.* 63 (1989) 2717.
25. C.James et al., *Phys.Rev.Lett.* 64 (1990) 843.
26. G.D.Barr et al., Proposal for a Precision Measurement of  $\epsilon'/\epsilon$  in CP Violating  $K^0 \rightarrow 2\pi$  decays, CERN/SPSC/90-22/ 253 (1990).
27. N.Doble et al., *Nucl.Instr.Meth.* B119 (1996) 181.
28. C.Biino, N.Doble, L.Gatignon, P.Grafstrom, H.Wahl, The Simultaneous Long and Short Lived Neutral Kaon Beams for Experiment NA48, Internal report: CERN-SL-98-033-EA (1998).
29. C.Biino, N.Doble, L.Gatignon, P.Grafstrom, H.Wahl, (Presented at EPAC-98, Stockholm, 22-26 June (1998); Preprint, CERN SL-98-041-EA (1998).
30. D.Bederede et al., *Nucl.Instr.Meth.* A367 (1995) 88; I.Augustin et al., *Nucl.Instr.Meth.* A403 (1998) 472.

31. G.D.Barr et al., *Nucl.Instr.Meth.* A370 (1996) 413.
32. B.Hallgren et al., *Nucl. Instr. and Meth.* A419 (1988) 680-685.
33. M.Holder, Status of the NA48 experiment. Proceedings of Workshop on Kaon Physics, Orsay (Edited by L. Iconomidou-Fayard, Editions Frontieres, 1996) 77.
34. I.Augustin, The NA48 experiment for the measurement of  $\epsilon'/\epsilon$ . Proceedings of the 28th International Conference on High Energy Physics, Warsaw, Poland (1996) 1679.
35. U.Koch, Doctoral Thesis, Universität Mainz, Nov. 1998